Modal Amplitude and Phase Estimation of Multimode Near Field Patterns Based on Artificial Neural Network with the Help of Grey-Wolf-Optimizer

Author names and affiliations:

Naoto Sugawara
Graduate School of Information Science and Technology, Hokkaido University
Sapporo 060-0814, Japan
sugawara@icp.ist.hokudai.ac.jp

Takeshi Fujisawa
Graduate School of Information Science and Technology, Hokkaido University
Sapporo 060-0814, Japan
fujisawa@ist.hokudai.ac.jp

Kodai Nakamura
Graduate School of Information Science and Technology, Hokkaido University
Sapporo 060-0814, Japan
nakamura@icp.ist.hokudai.ac.jp

Yusuke Sawada
Graduate School of Information Science and Technology, Hokkaido University
Sapporo 060-0814, Japan
sawada@icp.ist.hokudai.ac.jp

Takayoshi Mori
NTT Access Network Service Systems Laboratories, NTT Corporation
Ibaraki 305-0805, Japan
takayoshi.mori.sf@hco.ntt.co.jp

Taiji Sakamoto
NTT Access Network Service Systems Laboratories, NTT Corporation
Ibaraki 305-0805, Japan

taiji.sakamoto.un@hco.ntt.co.jp

Ryota Imada
NTT Access Network Service Systems Laboratories, NTT Corporation
Ibaraki 305-0805, Japan
ryota.imada.fh@hco.ntt.co.jp

Takashi Matsui
NTT Access Network Service Systems Laboratories, NTT Corporation
Ibaraki 305-0805, Japan
takashi.matsui.uh@hco.ntt.co.jp

Kazuhide Nakajima
NTT Access Network Service Systems Laboratories, NTT Corporation
Ibaraki 305-0805, Japan
kazuhide.nakajima.gr@hco.ntt.co.jp

Kunimasa Saitoh
Graduate School of Information Science and Technology, Hokkaido University
Sapporo 060-0814, Japan
ksaitoh@ist.hokudai.ac.jp

Corresponding author:

Takeshi Fujisawa
Graduate School of Information Science and Technology, Hokkaido University
Sapporo 060-0814, Japan
fujisawa@ist.hokudai.ac.jp

Modal Amplitude and Phase Estimation of Multimode Near Field Patterns Based on Artificial Neural Network with the Help of Grey-Wolf-Optimizer

Naoto Sugawara,[1] Takeshi Fujisawa,[1] Kodai Nakamura,[1] Yusuke Sawada,[1] Takayoshi Mori,[2] Taiji Sakamoto,[2] Ryota Imada,[2] Takashi Matsui,[2] Kazuhide Nakajima,[2] and Kunimasa Saitoh,[1]

[1]Graduate School of Information Science and Technology, Hokkaido University, Sapporo, Japan
[2]NTT Access Network Service System Laboratories, Tsukuba, Ibaraki, Japan

Abstract

A simple and efficient method for estimating modal amplitude and phase of multimode near field patterns (NFPs) based on artificial-neural-network (ANN) with the help of the optimization method is proposed. The inferred amplitude and phase of measured NFPs based on ANN are refined by using a gray-wolf optimizer (GWO). By using the proposed method, the image correlation between reproduced and measured NFPs is improved without re-training of ANN, which is the most time-consuming part of ANN-based numerical modal decomposition technique. Numerical examples of three and six mode cases are presented for the estimation using simple ANN. For six-mode case, the correlation is greatly improved by using the optimizer. Finally, the estimation of the measured NFPs from three-mode exchanger and six-mode mode conversion grating is implemented, and 5% improvement in the correlation value is observed for six-mode case. The proposed method offers alternative way to improve the correlation without using elaborated ANN.

Keywords

Modal decomposition technique, Artificial neural network, Mode division multiplexing, Mode scrambler

1. Introduction

In recent years, mode division multiplexing (MDM) transmission attracts a lot of attention for expanding the transmission capacity. In MDM transmission, so-called differential mode delay and mode dependent loss deteriorate the receiver performance. To overcome these problems, a mode exchanging or mixing technique at a relay point between two few-mode fibers (FMFs) is useful [1]. In a mode-exchanger or mode

mixer, input modes are converted or mixed with other modes. So far, various mode-mixing devices, such as mode exchangers (mode Exs) and mode scramblers, have been demonstrated in various platforms, such as planar lightwave circuit (PLC) [2-6] and fiber-based long-period gratings [7-9].

In the mode mixers, the output is usually the mixture of multiple modes. To evaluate the experimental performance of the device, the estimation of modal amplitude and phase of the fabricated device is necessary. We call this method as modal decomposition (MD) method, hereafter. To estimate these quantities, various MD methods have been developed and they are divided into two categories: experimental MD [10-13] and numerical MD methods [14-19]. For experimental MD methods, very high precision results can be obtained, however, usually precisely adjusted optical interference setup is necessary to accurately estimate the modal amplitude and phase, leading to complex measurement system and time-consuming post-data processing. For example, a digital holography approach [12,13] can perform MD with very high accuracy, however, precise experimental setup is necessary together with the preparation of reference beam. On the other hand, numerical MD technique usually only require the measurement of NFP and far field pattern (FFP) from the output. From the measured NFP (and sometimes FFP), the modal amplitude and phase can be estimated by using iterative optimization algorithm, such as, Gerchberg-Saxton algorithm [14], stochastic parallel descent algorithm [15], and line search algorithm [16]. These approaches are simple compared with the experimental ones in terms of the measurement setup. However, as discussed in [16], the accuracy and computation time of MD of these iterative methods strongly depend on their initial values for modal amplitude and phase. Although good guess for initial values accelerates the convergence, it is difficult to obtain it.

For non-iterative approach, numerical MD methods based on ANN [17-19] have attracted much attention. Using the NFP of multimode system as the input, trained ANN can infer the amplitude and phase, almost instantaneously. Although the training time of ANN usually takes long time, the inference itself does not take time once the training is finished. In [17,18], an special ANN called VGG-16 [20] was used to decompose the modes of FMF up to six modes. In [19], an special ANN called Dense-Net [21] was used to apply the method for large number of modes and ten-mode decomposition contained in 55-mode multimode fiber was demonstrated. In these articles, numerically calculated modal fields are randomly mixed and the mixed fields were used as training data. ANN was trained with the calculated NFPs and very high precision training was demonstrated by using special ANNs. However, if the method was applied to “measured” NFPs, the accuracy is degraded for large number of modes. For example, in [18], the averaged correlation value between numerically calculated and inferred NFPs was 0.9842 for six-modes. However, for the measured NFPs, the value is reduced to 0.8896. To increase the accuracy, the ANN has to be trained again

with including the measured data as additional training data. Since the most time-consuming part of numerical MD technique is the training part of ANN, it is not desirable to train ANN multiple times. Recently, an analytical MD method was proposed based on the calculation of pseudoinverse matrix [22]. The method is fast and accurate, however, it is also demonstrated that the error (phase error, especially) is increased for large number of modes and images with large noises. For both ANN and analytical approaches, further refinement of the estimation is difficult as in the iterative approach. In [23], a hybrid approach based on ANN and an optimization method was proposed. The training data was divided into 10 categories according to their shape, and the ANN was used as a classifier. If the image is inputted to the ANN, the label of the image is obtained. According to the label, the correlation values between the image and the training data belong to the same label were calculated, and amplitude and phase coefficients of the training data with maximum correlation are used as the initial guess of the optimization method. These values are refined by the interior point algorithm. The image reconstruction of three mode case was demonstrated, and the method seems to be very effective. However, as shown in [17-19] and this paper, the amplitude and phase coefficients can be learned directly in ANN, and therefore, the above process can be shortened. Also, generally speaking, since the interior point algorithm find a minimum based on gradient-based search, the gradient of the unknown function has to be calculated.

In this paper, to solve these problems, a simple and efficient MD method for estimating modal amplitude and phase of multimode NFPs based on ANN with the help of the optimization method is proposed. The amplitude and phase coefficients are directly learned with ANN and only the inferred phase of measured NFPs is refined by using a GWO, which is a meta-heuristic optimization algorithm [24]. Different from the gradient-based optimization, the GWO does not need any gradient calculations, and good exploitation and local minima avoidance characteristics were demonstrated [24]. By using the proposed method, the image correlation between reproduced and measured NFPs is improved without re-training of ANN. Furthermore, as shown later, the majority of errors comes from the phase error, and therefore, we only refine phase values in the iterative approach, reducing the variables for optimization half compared with [23]. Numerical examples of three and six mode cases are presented for the estimation using simple ANN. In addition to our preliminary conference report [25], detailed theoretical design and new experimental results are added in this paper. For the six-mode case, the correlation is greatly improved by using the optimizer. Finally, the estimation of the measured NFPs from three-mode EX [2] and six-mode mode conversion grating [6] based on PLC is implemented, resulting in 5% improvement in the correlation value for the six-mode case. The calculation time of the proposed approach is inferior to high-speed characteristics of non-iterative approach. However,

for some applications, such as simple device characterization shown in this paper, the accuracy is more important than the decomposition speed.

2. Theory

We consider the mixture of three or six modes in FMF as shown in Fig. 1. The mixed trasnverse field $\phi(x,y)$ can be expressed as

$$\phi(x,y)=\sum_{k=0}^{N-1} c_k \phi_k(x,y) e^{-j\theta_k} \quad (1)$$

where, N is the number of modes, c_k is the k-th modal amplitude with $\Sigma|c_k|^2 = 1$, $\phi_k(x,y)$ is the electric field of k-th each eigenmode, and θ_k is the modal phase, whose range is $[-\pi, \pi]$. Here, we set the phase of the fundamental mode $\theta_0 = 0$ and relative phases to the fundamental mode is treated. Therefore the goal of this paper is to estimate c_k and θ_k from given $\phi(x,y)$.

2.1 Learning with ANN

We use the simple ANN as shown in the left panel of Fig. 2 to estimate c_k and θ_k. The ANN is composed of input layer, output layer and multiple hidden layers. By renewing the weights of the nodes by an error back propagation method, the relationship between input and output characteristics are obtained. Here, the input layer is composed of the intensity (luminance) of NFP, in other words, pixel values of NFP image. In this paper, we use images with the resolution of $N_p \times N_p$, where N_p is the number of pixels for one row (or column) of the image. The output layer contains c_k and $\cos\theta_k$, and there are $2N$ -1 nodes. For the three-mode case, there are 5 nodes (three c_k and two $\cos\theta_k$) and for the six-mode case, there are 11 nodes (six c_k and five $\cos\theta_k$). The reason for using $\cos\theta_k$ instead of θ_k is that there are multiple combinations of the phase that give the same NFP, as shown in the right panel of Fig. 2 [17]. This deteriorates the learning of ANN. As shown later, the learning is more efficient if only the modal amplitude is treated. Both c_k and $\cos\theta_k$ are normalized to 0 to 1. The number of hidden layers is L-1, where L is the number of all layers except for the input layer. The number of nodes of i-th hidden layer is $N_{hd,i}$ (i = 1 to L-1). A sigmoid function is used for all the activation functions. No other special techniques, such as ReLU function, drop out, normalization, etc, are used. The initial values of weight of each node is given by Normal distribution with the standard deviation of $\sqrt{N_{NFP}}$, where N_{NFP} is the number of sample data. The values of weights are renewed based on steepest descent method.

We generate N_{NFP} randomly mixed data from the field of Fig. 1 by randomly generating c_k and θ_k. 90% of the data were used for training and remaining data were used for testing. The learning is evaluated by the average error given by

$$\delta=\sum_{i}^{t_N}\sum_{k}^{2N-1}\frac{\left|O_{ANN,ik}-O_{train,ik}\right|}{t_N(2N-1)} \quad (2)$$

where t_N is the number of testing data, $O_{train,ik}$ is the normalized c_k and $\cos\theta_k$ of i-th test data. $O_{ANN,ik}$ is the output values of trained ANN (normalized c_k and $\cos\theta_k$) for i-th test data input. Also, the correlation value C of two images is defined as [17]

$$C = \frac{\sum_{j=1}^{N_p}\sum_{i=1}^{N_p}\left(I_r(i,j)-\bar{I}_r\right)\left(I_m(i,j)-\bar{I}_m\right)}{\sqrt{\left(\sum_{j=1}^{N_p}\sum_{i=1}^{N_p}\left(I_r(i,j)-\bar{I}_r\right)^2 \cdot \sum_{j=1}^{N_p}\sum_{i=1}^{N_p}\left(I_m(i,j)-\bar{I}_m\right)^2\right)}} \tag{3}$$

where I_m, $\bar{I}_m$ are the luminance and average luminance values of inputted images, I_r, $\bar{I}_r$ are the luminance and average luminance values of ANN-reconstructed images. The range of the C is [0,1], and C = 1 if two images are perfectly equal. Since we learn $\cos\theta_k$ for the phase, there are two candidates for θ_k. Therefore, there are 2^{N-1} candidates for the phase combination. We calculate C for each set of the phase and choose the phase set having the largest C.

2.2 Phase estimation using GWO

By using the ANN described in the previous section, we can estimate c_k and θ_k from given $\phi(x,y)$. However, the accuracy of learning strongly depends on the architecture of the ANN, and for large number of modes, the accuracy is degraded [22]. Furthermore, as stated in the Introduction, if the "measured" image is input to the ANN, the correlation between the measured and estimated images tends to be low [18]. If we only use the ANN for the estimation, the only thing we can do is to train the ANN again with adding the new training data. The learning is the most time-consuming part in the ANN-based numerical MD technique, the alternative way to increase the accuracy is desired.

Here, we achieve this goal by using GWO [23]. The GWO is one of the optimizing algorithms mimicking the hunting of grey wolves. The flowchart of the algorithm is summarized in Fig. 3. There are N_w wolves and the position of i-th wolf is denoted by vector $\boldsymbol{X}_i$. The dimension of $\boldsymbol{X}_i$ corresponds to the search space of wolves. Each wolf has a fitness value according to the position, and large fitness means that the wolf is near the prey. The position is renewed by the positions of three wolves, α, β, and δ, who have top 3 fitness. At the iteration t, random vectors $\boldsymbol{A}_i$ and $\boldsymbol{C}_i$ are initialized as

$$\boldsymbol{A}_i = 2a\boldsymbol{r}_i - a \tag{4}$$

$$\boldsymbol{C}_i = 2\boldsymbol{r}_i \tag{5}$$

where $a = 2\text{-}2t/N_{it}$, N_{it} is a total iteration count and $\boldsymbol{r}_i$ is a random vector. Then, the fitness of all wolves are evaluated by their positions $\boldsymbol{X}_i$. In this paper, the fitness and the position correspond to the correlation value, C, and the phase set of mixed mode fields, θ_k as denoted in Fig. 3. Therefore, the dimension of $\boldsymbol{X}$ is N-1. From the fitness values, top 3 wolves are selected, and their positions are $\boldsymbol{X}_\alpha$, $\boldsymbol{X}_\beta$, $\boldsymbol{X}_\delta$. From these positions, following vectors are calculated.

$$\boldsymbol{X}_{1,i} = \boldsymbol{X}_{\alpha} - \boldsymbol{A}_i \circ \boldsymbol{D}_{\alpha,i} \tag{6a}$$

$$\boldsymbol{X}_{2,i} = \boldsymbol{X}_{\beta} - \boldsymbol{A}_i \circ \boldsymbol{D}_{\beta,i} \tag{6b}$$

$$\boldsymbol{X}_{3,i} = \boldsymbol{X}_{\delta} - \boldsymbol{A}_i \circ \boldsymbol{D}_{\delta,i} \tag{6c}$$

where $\circ$ denotes Hadamard product. $\boldsymbol{D}_{\mathrm{n}}$ is given by

$$\boldsymbol{D}_{n,i} = \left| \boldsymbol{C}_i \circ \boldsymbol{X}_n - \boldsymbol{X}_i \right| \tag{7}$$

where n = α, β, and δ. Then, the position of i-th wolf is renewed as

$$\boldsymbol{X}_i^{t+1} = \left(\boldsymbol{X}_{1,i} + \boldsymbol{X}_{2,i} + \boldsymbol{X}_{3,i} \right) / 3 \tag{8}$$

where the superscript shows the iteration count.

3. Numerical results for three- and six-mode case

Here, numerical examples of the estimation is presented. First, we consider three-mode case. We generate N_{NFP} = 10,000 images with a resolution of 64 × 64 (N_{p} = 64, the number of input nodes is 4,096). N_{p} is determined to match the measured NFPs, shown in section 4 later. 9,000 images are used for training and remaining 1,000 images are used for testing. First, we train ANN with only modal amplitude to show the difficulty of the estimation of the phase. For the amplitude estimation, the number of nodes of the output layer is 3. The left panel of Fig. 4 shows the learning curve and averaged C of ANN with L = 4 when only c_{k} is learned. We calculate the averaged C between the reproduced patterns by ANN and test patterns. For the phases, we used answer values. The learning curve is smooth and after training, δ is decreased to below 1%, and averaged C is over 0.999. It's shown that the amplitude can be estimated almost perfectly. Next, we estimate both modal amplitude and phase. The right panel of Fig. 4 shows the learning curve of c_{k} and θ_{k} for different number of ANN layers. By increasing the number of layers, δ is reduced and it is about 2% for L = 4. The training time for this ANN (N_{p} = 64) was 4 hours in our environment. From these results, the learning of modal amplitude only is easier than that of modal amplitude and phase. However, for the three-mode case, the error is small enough even if the phase is included in the learning.

Figure 5 shows the total calculation time of various approaches as a function of the number of pixels for three-mode case in our environment (Intel(R) Xeon(R) CPU E5-2630 v4 @ 2.20GHz, no parallelization technique is used). The dashed line shows the calculation time for forward propagation in ANN. The green solid line shows the calculation time for reproducing one image with phase estimation, explained in section 2.1. The calculation time is monotonically increased for the number of pixels and the time for forward propagation is very small. The red solid line shows the calculation

time for reproducing one image with 100 epoch in the GWO with $N_w = 4$ (If we use a parallelization in terms of wolves, the values will be $1/N_w$). If we use the GWO for the refinement of phase coefficients, the calculation time is further increased. However, as shown later for six-mode case, the accuracy is greatly improved. Therefore, the method is attractive for specific applications, where the accuracy is more important than the speed. Device characterizations, such as mode mixers shown in section 4, are one of the candidates.

Next, we consider six-mode case. We generate N_{NFP} = 100,000 images with a resolution of 90 × 90 (N_p = 90, the number of input nodes is 8,100). 90,000 images are used for training data and remaining 10,000 images are used for testing. The left panel of Fig. 6 shows the learning curves for six-mode case. A dashed line shows the learning curve when only the amplitude is learned for $L = 3$. The error is below 2% and high accuracy estimation is possible with simple ANN. Solid lines show the learning curves for c_k and θ_k for different number of ANN layers. The error is reduced with the epoch and ANN with $L = 3$ (2 hidden layers) shows the best performance in this case. The training time for this ANN (N_p = 90) was 108 hours in our environment. However, there are still 8% errors, showing the difficulty of estimating the phase from the intensity pattern only. The right panel of Fig. 6 show the learning curves for different N_{NFP}. For each N_{NFP}, 10% of data is used as test data. Although δ is decreased for large N_{NFP}, the accuracy is not so improved due to the difficulty of phase estimation. As shown in [17-19], by using special ANN based on convolutional network, the error can be reduced further. However, in this paper, since we want to show the accuracy improvement based on alternative technique, we use simple ANN.

To improve the image correlation without re-training of ANN, we use GWO described in 2-2. After estimating c_k and θ_k by using ANN, only θ_k are refined based on GWO. Here, we choose $N_w = 32$ and the initial positions of wolves are set to all phase sets given by the combinations of θ_k. From the test data, we take three images with worst C value (No.1) and not so good C values (No.2 and 3). These original images are shown in the left panel of the bottom panel of Fig. 7. The top panel of Fig. 7 shows C values of these three images reproduced by ANN or ANN+GWO. For the ANN, we use the ANN with $L = 3$. The leftmost bars show C values reproduced by ANN. If we use ANN only approach, the C value for No.1 is only 0.75. C values for No. 2 and 3 are 0.9 and 0.87. By using the phase set given by ANN, we estimate the true phase set by using the GWO. The bars of second from the left shows C values reproduced by ANN+GWO. The epoch is 100. By using GWO, the C values are greatly improved, and they are 0.984, 0.958 and 0.966 for No.1, 2, and 3. The reproduced images are shown in the third column in the bottom panel of Fig. 7.

Next, we investigate the characteristics of ANN+GWO under the noise. We add noises to original images with the signal to noise ratio (SNR). Here, SNR is defined as

$$SNR\ [\mathrm{dB}] = 10\log_{10}\left(\frac{I_{\max}}{I_{noise,\max}}\right) \tag{9}$$

where $I_{\max}$ is the maximum luminance value of the image and $I_{\mathrm{nosei,max}}$ is the maximum luminance noise. The luminance values of the pixels of the image with noise, I_{noise}, are given by

$$I_{noise}(i,j) = I(i,j) + 10^{\frac{-SNR}{10}} rand() \tag{10}$$

where I is the luminance value of the original image and $rand()$ is random number between 0 and 1.

The fourth column of the bottom panel of Fig. 7 shows the noise added images with SNR = 10 dB. The third and forth bars in the top panel of Fig. 7 shows C values reproduced images by ANN+GWO with SNR = 20 and 10 dB. Basically, the C values are worse when the noise is added. However, the C values are still greatly larger than those obtained by ANN reproduced images, showing the usefulness of the ANN+GWO approaches.

The calculation time of GWO for one wolf is about 1.0 ms for N_{p} = 90 in our environment described above. Therefore, if a parallel computation is implemented in terms of wolves, the total estimation time is about "1.0 ms × epoch of GWO" and the time required for GWO is not so long. However, compared with non-iterative approaches, the proposed method takes long time due to the GWO calculation.

The left panel of Fig. 8 shows the percentage of test data (Occupancy) as a function of error in terms of C for three-mode case. Orange and blue bars are for ANN and ANN+GWO. The interval of horizontal axis is 0.1%. For example, the percentage at a horizontal value of 0.05 means that the percentage of the test data between the error of 0 to 0.1%. For ANN+GWO, the phase values of each image speculated by ANN are refined based on GWO. GWO iteration is 100. For three-mode case, as shown in Fig. 4, since the accuracy of ANN is already high enough, the difference between two methods is small. The right panel of Fig. 8 shows the percentage of test data as a function of error in terms of C for six-mode case. The interval of horizontal axis is 2.5%. For ANN, the percentage between 0 to 2.5% error is 70%. The value is increased to 97.5% after the phase refinement by GWO. Therefore, C values using ANN+GWO is greatly improved compared with those of ANN.

4. Estimation of measured NFP

Here, we show the modal amplitude and phase estimation of "measured" NFP. We measured output NFPs of FMF-pigtailed PLC modules. For three-mode case, output NFPs of three-mode EX [2] are examined. For six-mode case, output NFPs of mode conversion gratings [6] are examined.

4.1 NFPs of three-mode EX based on PLC

Figure 9 shows a schematic of three-mode EX. The device was fabricated on silica-PLC platform. The device consists of cascaded adiabatic directional coupler, directional coupler, and mode rotator, which converts inputted LP_{11a} mode to LP_{11b} mode. The device is designed to exchange modes as shown in the right panel of Fig. 8. The detail of the device operation principle can be found in [2]. FMF-pigtailed module is made by using the fabricated chip and shown in the left picture of Fig. 10. We measured the output NFPs by launching LP_{01}, LP_{11a}, and LP_{11b} modes at 1550 nm from the input side and they are shown in the right panel of Fig. 10. Launched LP_{01} mode is converted to two peak LP_{11}-like mode, as expected. The mode power ratio of the output light for LP_{01} input is measured by a bending method [26]. Since $LP_{11a,b}$ components are easily coupled each other in the pigtailed FMF, we cannot discriminate these modes. Therefore, we only measure the power ratio between LP_{01} and $LP_{11a,b}$ modes. The power ratios for LP_{01} and $LP_{11a,b}$ modes are 34 and 66 %, showing majority of the power is converted to $LP_{11a,b}$ mode. Similarly, the power ratios for $LP_{11a,b}$ inputs were measured and they are 0.48:0.52 for LP_{11a}, and 0.12:0.88 for LP_{11b} input. These values are summarized in Table 1. The next task is to reproduce these images. Figure 11 shows the reproduced images of three-mode EX based on ANN (left) and ANN+GWO (right). Here, the number of wolves is 12, and initial positions (corresponding to the phase set) of 4 wolves are set to the combinations of the phase set speculated by ANN and the positions of remaining 8 wolves are set to random values. Although the number of wolves has a little effect to the C value if $N_w > 2^{N-1}$, we increased N_w for large space exploitation. The iterations of GWO are 100. Numbers shown below the images are C between measured and reproduced images. Measured images are successfully reproduced with large values of C. In this case, the difference between two methods is small. In Table 1, the power ration between LP_{01} and $LP_{11a,b}$ modes calculated by the reproduced images are also shown, and they are in very good agreement with the measured results, showing the accuracy of the reproduced images.

4.2 NFPs of six-mode mode conversion gratings based on PLC

Figure 12 shows a schematic of the mode conversion gratings [6]. One side of the waveguide is periodically corrugated to convert input mode to the different mode. The pitch, the depth, and the length of the grating waveguide are Λ, d, and L, respectively. Here, we consider two grating waveguides (Grating-1: G1, Grating-2: G2). In G1, two mode sets (E_{11}-E_{12} and E_{21}-E_{22}) are simultaneously converted. In G2, E_{11} mode is converted to E_{31} mode. The BPM simulated fields are shown at the right side of Fig. 12. The details of these grating can be found in [5,6].

To reproduce the images, we use ANN with $L = 3$ and $N_{NFP} = 100{,}000$ in Fig. 6. For GWO, we set $N_w = 50$, and initial positions of 32 wolves are set to the combinations of the phase set speculated by ANN and remaining 18 wolves are set to

random. The top panel of Fig. 13 and 14 are measured NFPs of G1 and G2. The input mode for each NFP is written below the image. Strongly mixed NFPs can be seen. The middle panel of Fig. 13 and 14 are reproduced images by ANN. The values below the images are correlation values. The averaged correlations are 0.93 and 0.91 for G1 and G2.

To increase the accuracy, we use ANN+GWO. The left and right panels of Fig. 15 shows *C* values as a function of GWO iterations for G1 and G2. The *C* values for each input mode is improved with GWO iterations. The bottom panel of Fig. 13 and 14 show reproduced images by ANN+GWO. The values below the images are correlation values. If the *C* value obtained by ANN is already large, the improvement is not so large. However, if it is small, the improvement is significant. For example, the worst *C* value obtained by ANN is 0.844 for LP_{02} input of G2. It is improved to 0.93 by using ANN+GWO, almost 10% increase in the *C* value. The averaged correlations are 0.95 and 0.96 for G1 and G2. These values are summarized in Table 2. The correlations are clearly improved, especially for LP_{11a} and LP_{02} input, showing the usefulness of the proposed method. Remaining errors may come from the existence of radiation modes in the NFPs, which is not taken into account in the theory.

5. Conclusion

A novel method for estimating modal amplitude and phase of multimode NFP is proposed. The method is based on ANN with the help of optimizer for the phase estimation. The method is effective when the accuracy of the speculation based on ANN is not enough and offer alternative way to improve the image correlation. Measured NFPs of recently proposed three- and six-mode devices are successfully reproduced, showing the usefulness. The proposed approach is useful for applications, where the accuracy is more important than decomposition speed. Although we used simple ANN in this paper, one can use, of course, more elaborated ANN, such as convolutional NN, or other non-iterative approach, such as an analytical MD method [22].

References

[1] Y. Wakayama, D. Soma, K. Igarashi, H. Taga, and T. Tsuritani, “Intermediate mode interchange for reduction of differential mode-group delay in weakly-coupled 6-mode fiber transmission line,” in Proc of OFC 2016, M3E.6 (2016).

[2] T. Fujisawa, E. Taguchi, T. Sakamoto, T. Matsui, Y. Yamashita, K. Tsujikawa, K. Nakajima, and K. Saitoh, “One chip, PLC three-mode exchanger based on symmetric and asymmetric directional couplers with integrated mode rotator,” in Proc of OFC 2017, W1B.2 (2017).

[3] T. Fujisawa, Y. Yamashita, T. Sakamoto, T. Matsui, K. Tsujikawa, K. Nakajima, and K. Saitoh, "Scrambling-type three-mode PLC multiplexer based on cascaded

Y-branch waveguide with integrated mode rotator", J. Lightwave Technol., **36**, 1985-1992 (2018).

[4] M. Shirata, T. Fujisawa, T. Sakamoto, T. Matsui, K. Nakajima, and K. Saitoh, " A design of small mode-dependent-loss scrambling-type mode (de)multiplexer based on PLC," Opt. Express, **28**, 9653-9665 (2020).

[5] M. Shirata, T. Fujisawa, T. Sakamoto, T. Matsui, K. Nakajima, and K. Saitoh, "A design of PLC-based 6-mode exchanger in mode division multiplexed transmission," in Proc of IPC 2019, TuH1.4 (2019).

[6] T. Fujisawa, T. Sakamoto, M. Miyata, T. Matsui, T. Hashimoto, R. Kasahara, T. Mori, R. Imada, K. Nakajima, and K. Saitoh, "Six-mode scrambler based on cascaded side-wall grating waveguides", Jpn. J. Appl. Phys., **60**, 062002 (2021).

[7] B. Huang, H. Chen, N.K. Fontaine, R. Ryf, I. gailes, and G. Li, "Large-bandwidth low-loss, efficient mode mixing using long-period mechanical gratings" Opt. Lett., **42**, 3594-3597 (2017).

[8] H. Chen, N.K. Fontaine, B. Huang, R. Ryf, and I. Gailes, "Demonstration of mode scramblers supporting 6 spatial modes to reduce differential group delays" in Proc of ECOC 2017, W2F3 (2017).

[9] Y. Zhao, H. Chen, N.K. Fontaine, J. Li, R. Ryf, and Y. Liu, "Broadband and low-loss mode scramblers using CO2-laser inscribed long-period gratings," Opt. Lett., **43**, 2868-2871 (2018).

[10] J. Carpenter, B. C. Thomsen, and T. D. Wilkinson, "Degenerate mode-group division multiplexing," J. Light Technol. **30**(24), 3946–3952 (2012).

[11] J. W. Nicholson, A. D. Yablon, S. Ramachandran, and S. Ghalmi, "Spatially and spectrally resolved imaging of modal content in large-mode-area fibers," Opt. Express **16**(10), 7233–7243 (2008).

[12] T. Kaiser, D. Flamm, S. Schröter, and M. Duparré, "Complete modal decomposition for optical fibers using CGH-based correlation filters," Opt. Express **17**(11), 9347–9356 (2009).

[13] M. Lyu, Z. Lin, G. Li, and G. Situ, "Fast modal decomposition for optical fibers using digital holography," Sci. Rep. **7**(1), 6556 (2017).

[14] O. Shapira, A.F. Abouraddy, J.D. Joannopoulos, and Y. Fink, "Complete modal decomposition for optical waveguides," in Proc of CLEO, CThB2 (2005).

[15] H. Lu, P. Zhou, X. Wang, and Z. Jiang, "Fast and accurate modal decomposition of multimode fiber based on stochastic parallel gradient descent algorithm," Appl. Opt., 52, 2905-2908 (2013).

[16] R. Bruning, P. Gelszinnis, C. Schulze, D. Flamm, and M. Duparre, "Comparative analysis of numerical methods for the mode analysis of laser beams," Appl. Opt., **52**, 7769-7777 (2013).

[17] Yi An, L. Huang, J. Li, J. Leng, L. Yang, and P. Zhou, “Learning to decompose the modes in few- mode fibers with deep convolutional neural network,” Opt. Express, **27**, 10127–10137 (2019).

[18] Yi An, L. Huang, J. Li, J. Leng, L. Yang, and P. Zhou, “Deep learning-based real-time mode decomposition for multimode fibers,” J. Sel. Top. Quantum Electron., **26**, 440806 (2020).

[19] S. Rothe, Q. Zhang, N. Koukouakis, and J. Czarske, “Intensity-only mode decomposition on multimode fibers using a densely connected convolutional network,” J. Lightwave Technol., **39**, 1672-1679 (2021).

[20] K. Simonyan and A. Zisserman, “Very deep convolutional networks for large-scale image recognition,”, https://arxiv.org/abs/1409.1556.

[21] G. Huang, Z. Liu, L. Van Der Maaten, and K. Q. Weinberger, “Densely connected convolutional networks,” in Proc. IEEE Conf. Comput. Vis. Pattern Recognit*,* 4700–4708 (2017).

[22] E.S. Manuylovich, V.V. Dvoyrin and S.K. Turitsyn, "Fast mode decomposition in few-mode fibers," *Nat. Comm.,* 11(1), 1-9 (2020).

[23] H. Gao, H. Hu, Y. Zhao, and J. Li, “A real-time fiber mode demodulation method enhanced by convolution neural network,” Optical Fiber Technology **50**, 139-144 (2019).

[24] S. Mirjalili, S.M. Mirjalili, and A. Lewis, “Grey wolf optimizer,” Advances in Engineering Software, **69**, 46-61 (2014).

[25] N. Sugawara , T. Fujisawa, K. Nakamura, Y. Sawada, T. Sakamoto, T. Matsui, K. Nakajima, and K. Saitoh, "Mode amplitude and phase estimation of NFP of six-mode FMF based on artificial neural network with the help of grey-wolf-optimizer”, in Proc. of ECOC 2020, Tu2A-6 (2020).

[26] K. Nakanishi, H. Kubota, Y. Miyoshi, M. Ohashi, T. Sakamoto, T. Matsui, K. Nakajima, and F. Yamamoto, “Mode excitation ratio measurement of a two-mode fiber with offset fusion splice,” in Proc. IEEE Opto-Electron. Commun. Conf. 2015, PWe.43 (2015).

Figure captions

Fig. 1. Six mode fields of FMF.

Fig. 2. (Left) A schematic of ANN and (right) NFP candidates for the same set of cosine values of the phase set.

Fig. 3. A flowchart of GWO.

Fig. 4. (Left) Learning curves and the average C values for three-mode case when only the modal amplitude is taken into account. (right) Learning curves for both modal amplitude and phase.

Fig. 5. The calculation time as a function of the number of pixels for three-mode case.

Fig. 6. (Left) Learning curve of modal amplitude (dashed) and modal amplitude and phase (solid) for six-mode case. (Right) Learning curves for both modal amplitude and phase with different N_{NFP}.

Fig. 7. (Top) C values obtained by ANN and ANN+GWO approaches with and without noise for six-mode case. (Bottom) Test and reproduced images.

Fig. 8. The percentage of test data as a function of error in terms of C for (left) three- and (right) six-mode cases.

Fig. 9. A schematic of three-mode EX and its operation.

Fig. 10. (left) A picture of the fabricated module of three-mode EX and (right) measured NFPs of this module.

Fig. 11. Reproduced images of three-mode EX based on (left) ANN and (right) ANN+GWO. The numbers below Figures indicate C values between measured and reproduced images.

Fig. 12. (Left) A schematic of mode conversion grating and (right) BPM simulated field distributions of G1 and G2.

Fig. 13. (Top) Measured NFPs of G1. The input mode is denoted below the images. Reproduced images of G1 based on (middle) ANN and (bottom) ANN+GWO. The numbers below Figures indicate C values between measured and reproduced images.

Fig. 14. (Top) Measured NFPs of G2. The input mode is denoted below the images. Reproduced images of G2 based on (middle) ANN and (bottom) ANN+GWO. The numbers below Figures indicate *C* values between measured and reproduced images.

Fig. 15. *C* values as a function of GWO iterations for (left) G1 and (right) G2.

Table captions

Table 1. Measured and speculated power ratio between LP_{01} and LP_{11} modes of three-mode EX

Table 2 Averaged correlation values for G1 and G2

Figure 1

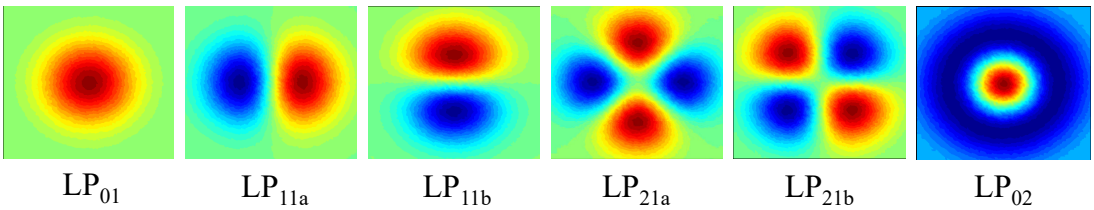

Figure 2

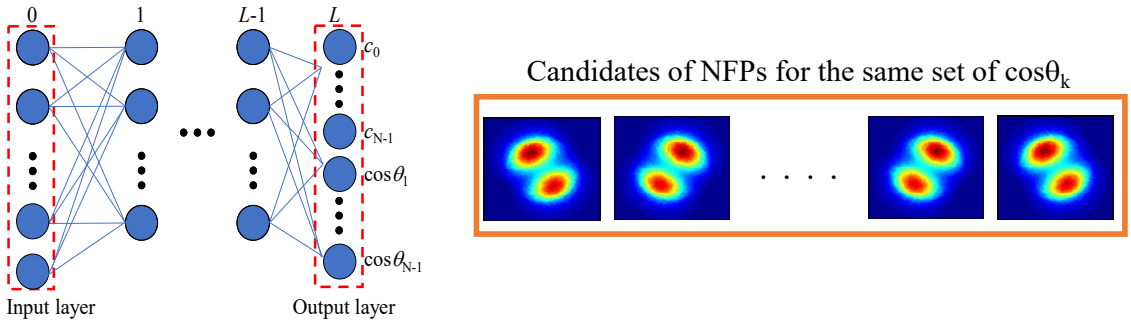

Figure 3

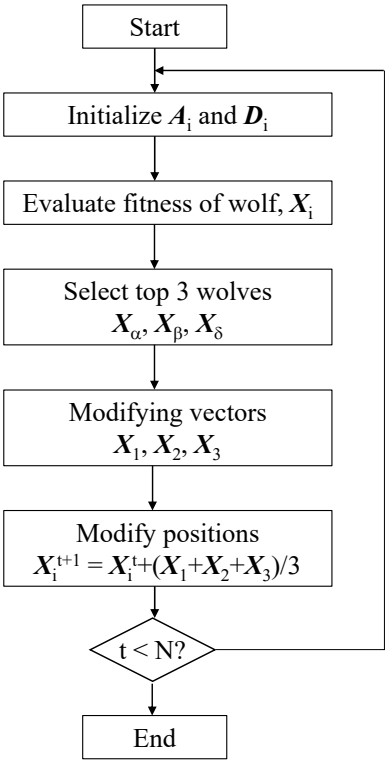

- N_w : The number of wolves
- $\boldsymbol{X}_i$: The position of i-th wolf
  i = 1 to N_w
- The dimension of $\boldsymbol{X}$ is N-1
  (The number of phase set)
- The fitness of each wolf is
  correlation value C

Figure 4

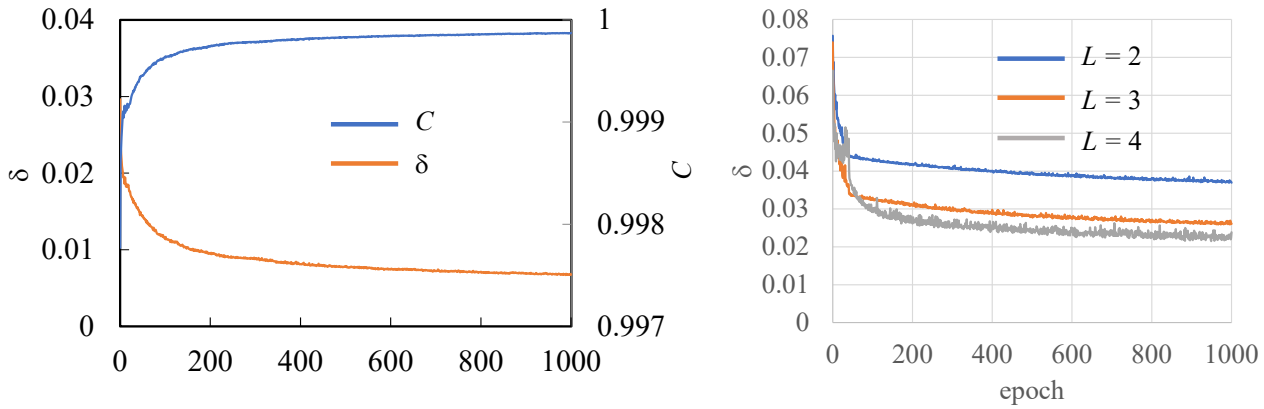

Figure 5

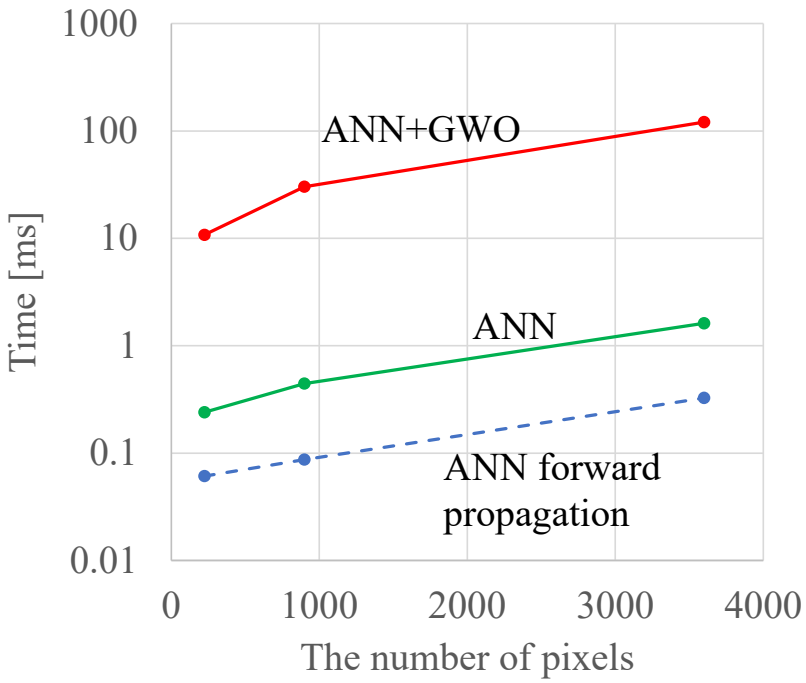

Figure 6

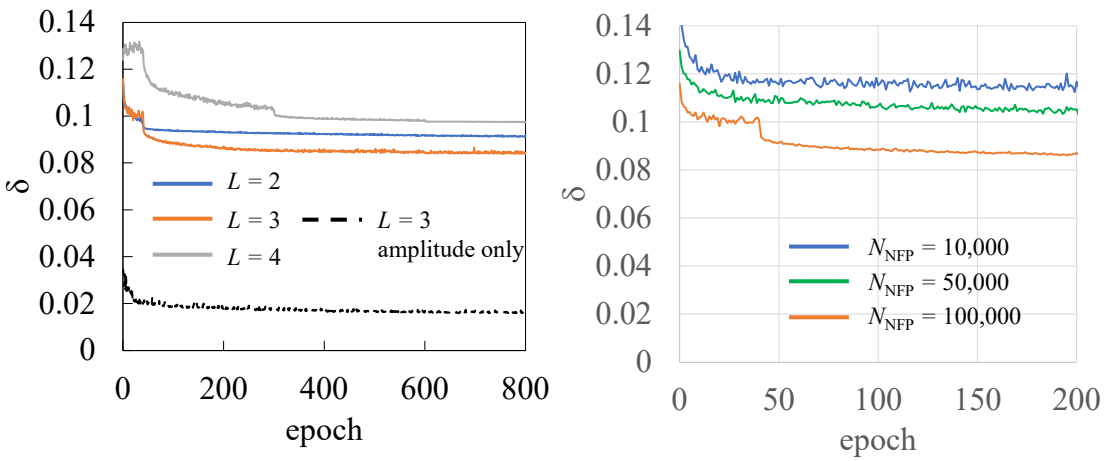

Figure 7

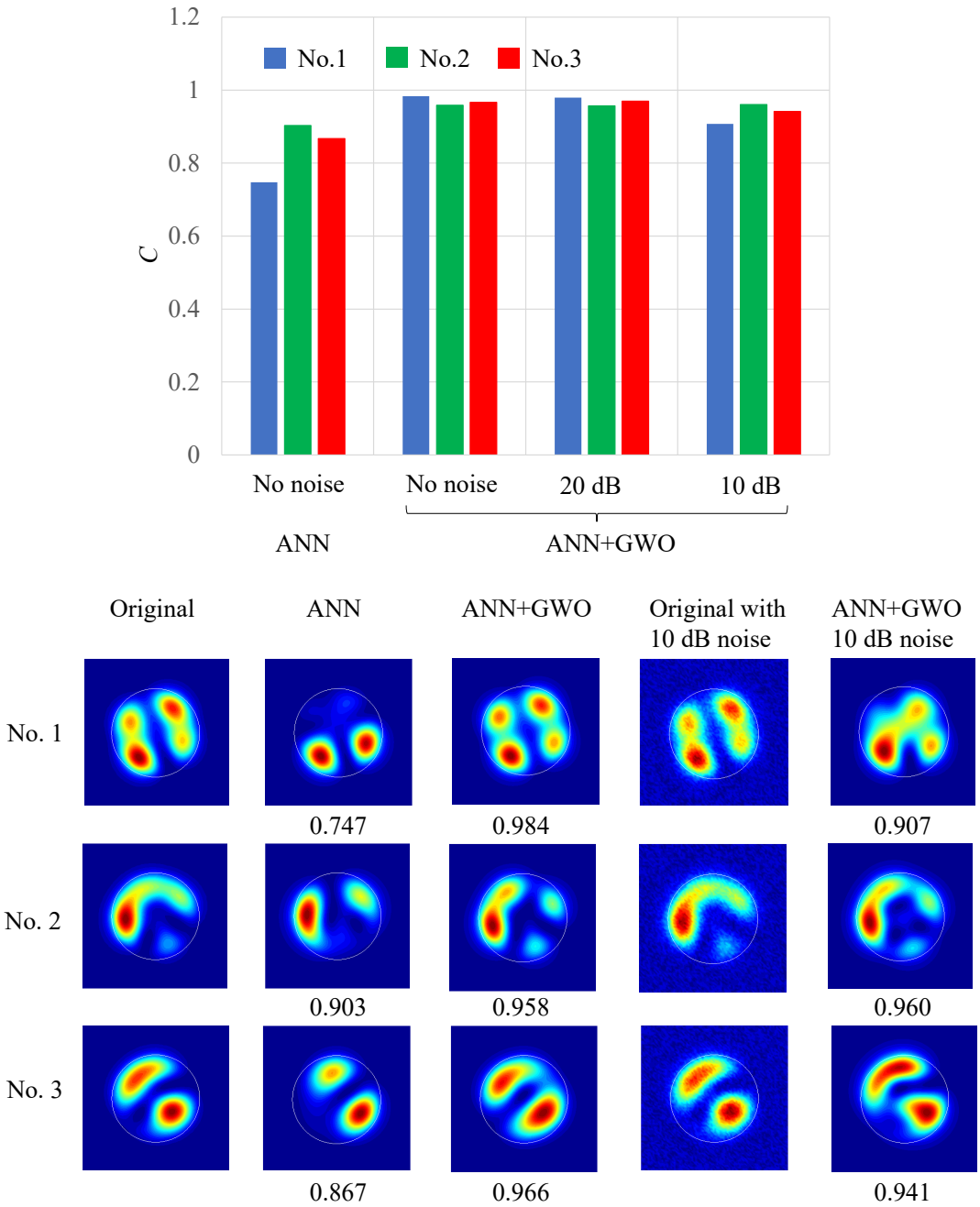
1.2
1
0.8
0.6
0.4
0.2
0
C
No.1
No.2
No.3
No noise
No noise
20 dB
10 dB
ANN
ANN+GWO
Original
ANN
ANN+GWO
Original with 10 dB noise
ANN+GWO 10 dB noise
No. 1
0.747
0.984
0.907
No. 2
0.903
0.958
0.960
No. 3
0.867
0.966
0.941

Figure 8

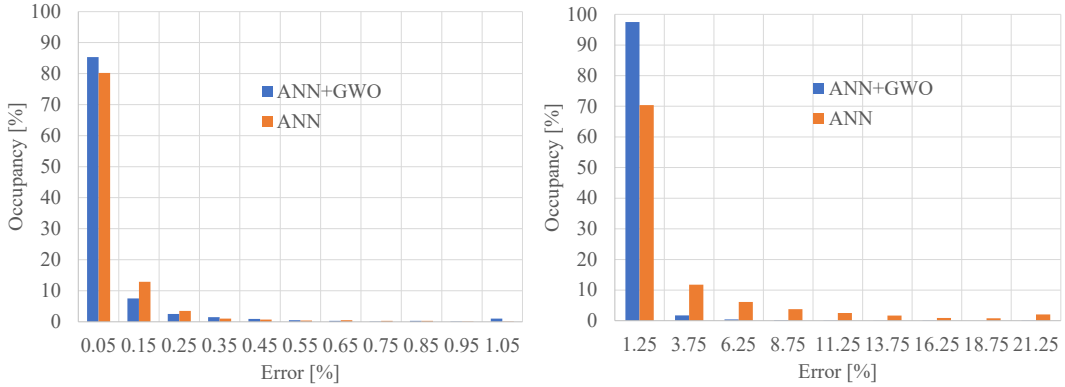

Figure 9

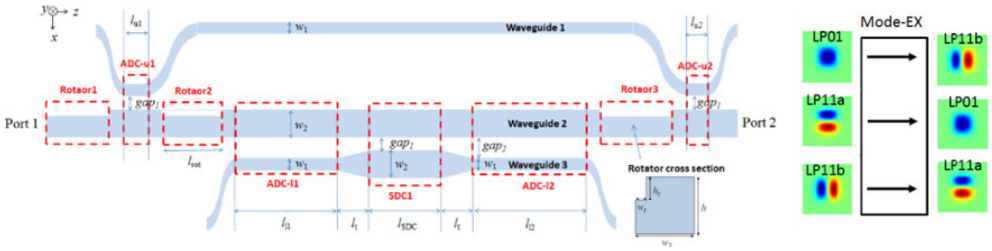

Figure 10

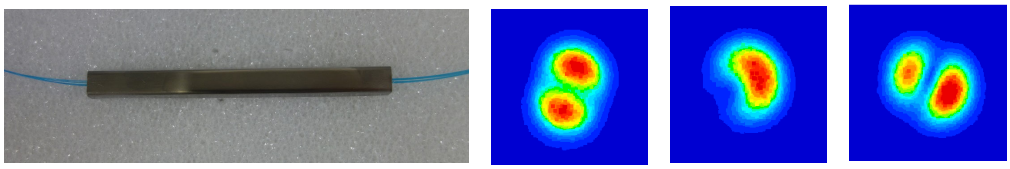

LP_{01} input LP_{11a} input LP_{11b} input

Figure 11

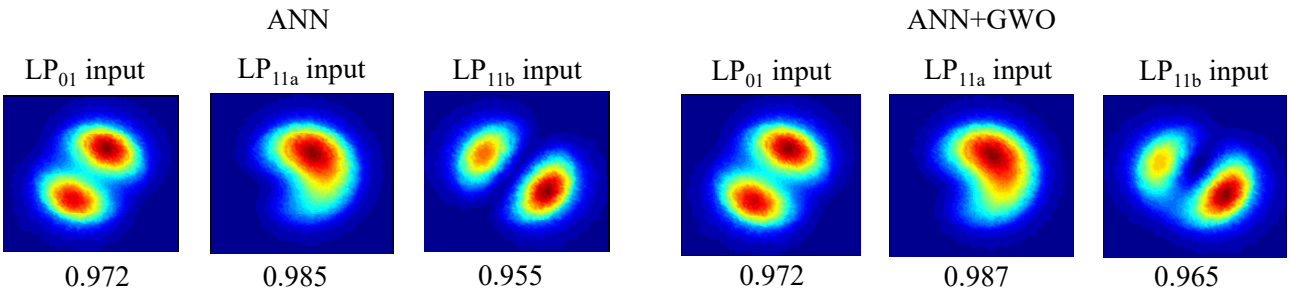

Figure 12

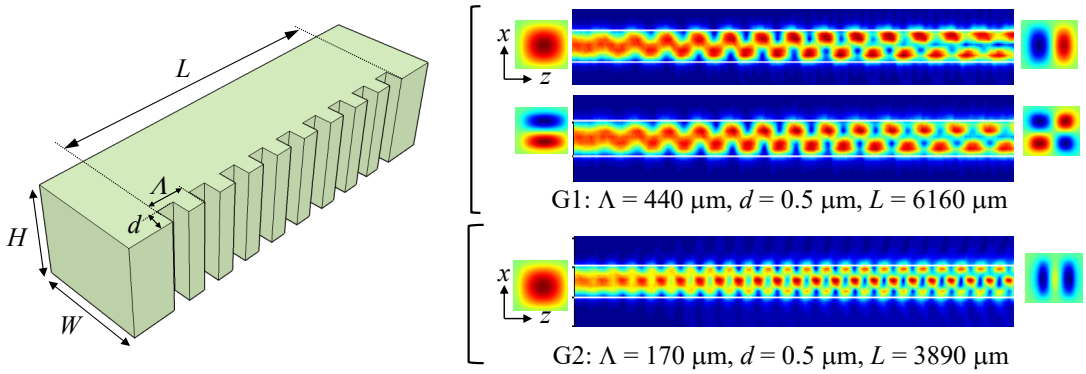

Figure 13

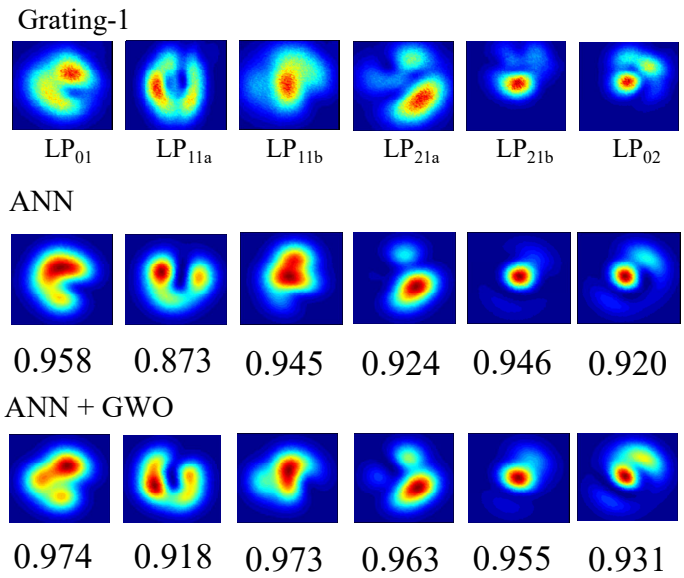

Figure 14

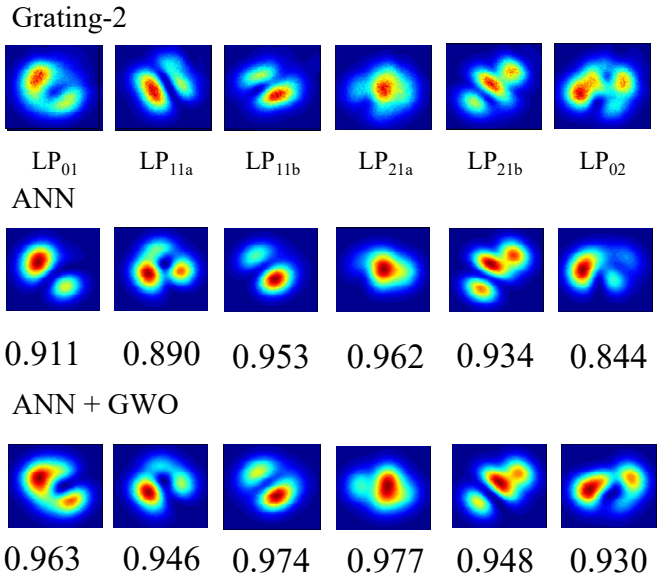

Figure 15

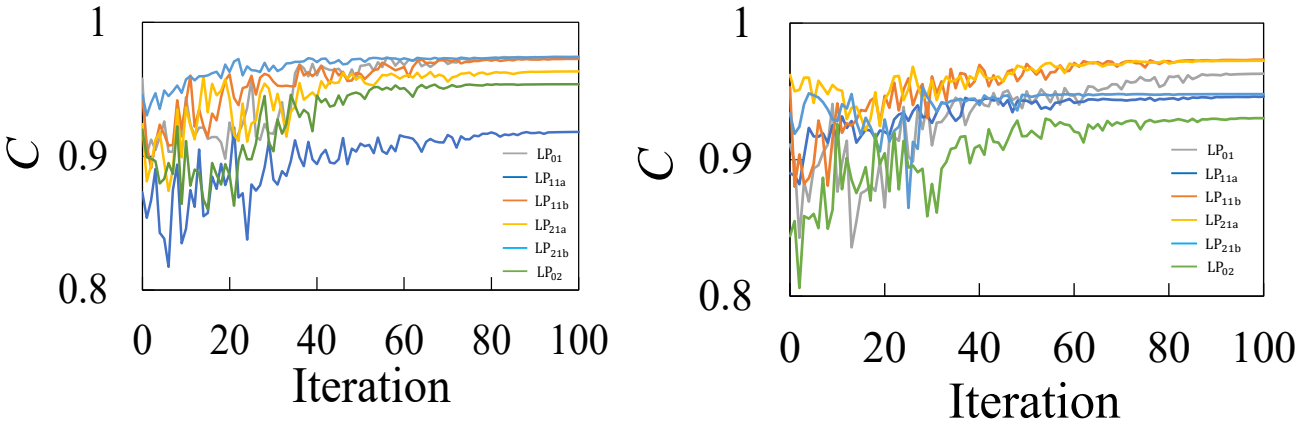

Table 1

Input mode	LP_{01}	LP_{11a}	LP_{11b}
Power ratio	LP_{01}:LP_{11}		
Bending method	0.36:0.64	0.48:0.52	0.12:0.88
ANN	0.35:0.65	0.47:0.53	0.15:0.85

Table 2

	G1	G2
ANN	0.93	0.91
ANN+GWO	0.95	0.96